AIAA SciTech
4-8 January 2016, San Diego, California, USA
AIAA Guidance, Navigation, and Control Conference

Attitude Stabilization of an Uncooperative Spacecraft in an Orbital Environment using Visco-Elastic Tethers

Kirk Hovell* and Steve Ulrich†
Carleton University, Ottawa, ON, K1S 5B6, Canada

Active removal of large de-commissioned satellites is critical to the continued use of many of Earth's orbits, as predicted by Donald J. Kessler in 1978. One solution to this problem is to use a tethered spacecraft system to capture and tow the highest risk debris to a disposal orbit. A significant technical challenge lies with the capture, and subsequent stabilization, of a large and possibly tumbling debris. This paper addresses the target attitude stabilization aspect of the capture process. The two systems analyzed consist of 1) the currently accepted tethered spacecraft system where a single tether joins the target and the active chaser spacecraft, and 2) a newly proposed tethered spacecraft configuration that consists of a single tether attached to the active chaser spacecraft, which branches into four sub-tethers attached to the debris. An orbital environment is simulated, including gravity gradient torques. Incorporating the thrust ability of the chaser and exploiting the visco-elastic properties of the tethers, it is shown through numerical simulations that the proposed novel tethered spacecraft configuration provides an improved means of controlling the attitude of an uncooperative debris.

Nomenclature

J	Inertia matrix, $\text{kg} \cdot \text{m}^2$
$\mathcal{F}_x$	Reference frame x
τ	Torque, N·m
F	Force, N
m	Mass, kg
ω	Angular rate, rad/s
q	Quaternion
s	Tether stretch, m
μ	Gravitational parameter, m^3/s^2
$\vec{r}$	Position vector, m
$\vec{v}$	Velocity vector, m/s
k	Spring constant, N/m
c	Damping coefficient, N·s/m
$\dot{x}$	Time derivative of x
$\vec{x}$	Vector x
$\mathbf{x}$	Three dimensional components of physical vector $\vec{x}$

Subscript

i	Variable number
t, j, c	Refers to target, junction, or chaser, respectively

Superscript

T	Transpose
b	Body frame
$\times$	Skew-symmetric matrix

*Graduate Student, Department of Mechanical and Aerospace Engineering, 1125 Colonel By Drive. Student Member AIAA.
†Assistant Professor, Department of Mechanical and Aerospace Engineering, 1125 Colonel By Drive. Senior Member AIAA.

I. Introduction

The density of Earth-orbiting debris has increased dramatically over the last decade. The highest risk debris are the largest (e.g., uncooperative decommissioned satellites), which, in the event of a collision have the potential to create many additional debris. It is foreseen that if the number of debris keeps increasing with the current growth rate, this will rapidly lead to an exponential growth in collisions, thereby reducing the availability of some orbits due to the higher risk of collision with orbiting space debris. This is referred to as the *Kessler Syndrome*.[1] In this context, controlling the growth of the large space debris population is a high-priority task of the world's major space agencies. A notable example is the e.Deorbit mission in development by the European Space Agency under its Clean Space initiative.[2]

To address this contemporary problem, several space debris mitigation approaches were recently proposed, such as capturing an uncooperative target with a harpoon,[3] a mechanical arm,[4] or a net.[5] An interesting deorbiting method is via electrodynamic tether.[6] This technique passively conducts current through a radial tether, which, through interaction with the geomagnetic field, produces a deorbiting thrust. This is a simple and reliable method for deorbiting a debris, and is currently under development. Another one of the most promising solutions consists of creating a tethered spacecraft system (TSS), i.e., an active chaser spacecraft capturing and deorbiting an uncooperative, and possibly spinning, target spacecraft (i.e., a space debris) using a viscous-elastic tether.[7] There are multiple techniques for establishing the TSS. Most notably, 1) deploying a net over the target which is tethered back to the chaser, or 2) launching a harpoon towards the target, that is tethered back to the chaser. Tethered spacecraft systems have the benefit of long deployment range and reduced mechanical complexity over that of a rigid connection. However, the use of tethered spacecraft systems to remove space debris from populated orbits involves several technical challenges. Those challenges are mostly related to the structural flexibility of the tether coupled with the large angular velocities of space debris that may exceed 30 rotations per minute.[8] For this reason, controlling the relative dynamics of the chaser spacecraft with respect to the target spacecraft, in such a way that the flexible tether reduces the angular momentum of the debris as much as possible, is critical to ensuring the success of the TSS debris-removal technological solution. Indeed, only once the angular momentum of the debris is regulated, can the chaser safely maneuver without risk of collision.

Tethered spacecraft systems are fairly common and are extensively used for extravehicular activity (EVA) and have been studied in depth.[9,10,11] A notable experiment is TSS-1R,[12] where a 20.7 km conductive tether with a spherical satellite on the end was reeled out of the Shuttle on STS-46. The goals were to test TSS models and determine the feasibility of TSS utilization in the future. However, in these studies, both objects, attached together by a tether, were treated as point masses. This is sufficient detail when each object has a means of controlling its own attitude (as is present during an EVA or most other applications). However, in the context of using one spacecraft to control a spinning and uncooperative space debris, a more detailed analysis on the attitude dynamics of the debris must be considered.

The effects a TSS has on an the attitude of an uncooperative target has only been recently studied. In Ref. 13, a Lagrangian approach was taken to model the planar two-dimensional dynamics of a single tether on a rigid passive target. Numerical simulations were performed for various cases, which demonstrated that a tether is feasible for controlling a passive target. It was found that a slack tether should be avoided, as it can yield high amplitude oscillations of the target attitude about its equilibrium.

The same authors then performed a Lagrangian approach to model the TSS effects on a rigid target with flexible appendages in two-dimensions[14] and again in three-dimensions.[15] It was found that the tether material properties (i.e., stiffness) must be selected such that it does not generate TSS oscillations that coincide with the natural frequencies of the target spacecraft when the flexible appendages are deployed.

Aerodynamic torques on a large space debris were separately considered,[16] with the conclusion that aerodynamic torques can alter the stability of the target during the deorbiting period, especially near disposal orbit altitudes below 300 km.

More recently, Aslanov and Yudintsev further modeled the TSS using a three-dimensional Newtonian approach.[17] More representative effects such as orbital motion, gravity-gradient torques, and atmospheric drag were included in the simulations. Certain configurations were shown to lead to safe transportation, such as when the single tether is aligned with the thrust vector of the chaser. It was found that sufficient levels of thrust force are required from the chaser, and this level increases as the altitude of the TSS decreases due to the increasing effect of atmospheric drag. Most notably, it was determined that tether damping only slightly reduces the attitude oscillations of the passive satellite. As a result, the target spacecraft will most likely be oscillating during the deorbiting period, possibly leading to control difficulties for the chaser.

In this context, this paper proposes a novel tethered spacecraft configuration to significantly improve the attitude stabilization ability of the TSS. The novel approach is to implement four sub-tethers attached to the debris at various locations to increase its attitude stability. A three-dimensional Newtonian modeling approach is taken, and the effects of flexible appendages are not considered. Dynamics formulations and simulations are presented for both the single tether configuration, previously proposed by Aslanov and Yudintsev,[17] modeled as well as the novel sub-tether approach to demonstrate the improved target stabilization performance of the novel approach. Similar to Ref. 17, orbital motion and gravity gradient torques are included.

The main contributions of this paper are: the presentation of a novel tethered spacecraft system concept where a main tether branches into four sub-tethers that are attached to the extremities of the target, the development of the equations of motion for the system that includes orbital motion, tether forces, and gravity gradient torques, and simulations demonstrating the improved target-stabilizing ability the novel tethered spacecraft system as compared to the previously-studied TSS models.

This paper is organized as follows: Sec. II describes the approach taken to solve the dynamics problem, Sec. III presents a dynamics formulation for the sub-tether configuration, Sec. IV presents the dynamics for a single tether configuration, Sec. V demonstrates the improved performance of the approach using numerical simulations, and Sec. VI summarizes the results.

II. Approach

The currently accepted tethered spacecraft system consists of an active satellite (chaser) connected to a debris (target) via a visco-elastic tether. Figure 1a shows a typical, previously-studied,[7,13–16] configuration. A tether connects the chaser to an attachment point on the target. The proposed configuration is shown in Figure 1b, and has a tether attached to the chaser which branches into four smaller tethers that are attached to the target at various locations. The single tether leaving the chaser will be denoted as the *main tether* and the four tethers connecting the main tether to the target are denoted as *sub-tethers*. The point where the main tether splits into sub-tethers is denoted the *junction*. Similarly to Refs. 7 and 13-16, the tethers are modeled as massless single links (i.e., no torsion or bending effects). The single tether is assumed to be perfectly attached to the debris the center of the front panel, as shown in Figure 1a, and the sub-tethers are assumed to be perfectly attached to the extremities of the front panel the debris, as shown in Figure 1b. The approach taken herein is to use the spring-damper properties of the main tether and sub-tethers to regulate the angular momentum of an uncontrolled target, in a low-Earth orbit environment. The purpose of this paper is to demonstrate how the proposed novel TSS provides an improved stabilizing ability compared to the currently available approach.

III. Dynamics Formulation - Sub-Tether Configuration

Referring to Figure 1b, the reference frame $\mathcal{F}_I$ represents an inertially fixed reference frame. The position of the target is described by position vector $\vec{r}_t$, such that:

$$\vec{r}_t = \vec{\mathcal{F}}_I^{\mathrm{T}} \mathbf{r}_t. \tag{1}$$

where, $\mathbf{r}_t$ represents the three-dimensional components of the target center of mass vector in the inertially fixed reference frame $\mathcal{F}_I$. The junction and chaser are represented as point masses, their locations described by position vectors $\vec{r}_c$ and $\vec{r}_j$, respectively, such that:

$$\vec{r}_c = \vec{\mathcal{F}}_I^{\mathrm{T}} \mathbf{r}_c \tag{2}$$

$$\vec{r}_j = \vec{\mathcal{F}}_I^{\mathrm{T}} \mathbf{r}_j \tag{3}$$

where $\mathbf{r}_c$ and $\mathbf{r}_j$ are the three-dimensional components of the chaser and junction vectors in the inertially fixed reference frame $\mathcal{F}_I$, respectively.

A. Attitude motion

Euler's equations of motion are used to describe the target angular rates in the target body-fixed reference frame $\mathcal{F}_B$, given by:[18]

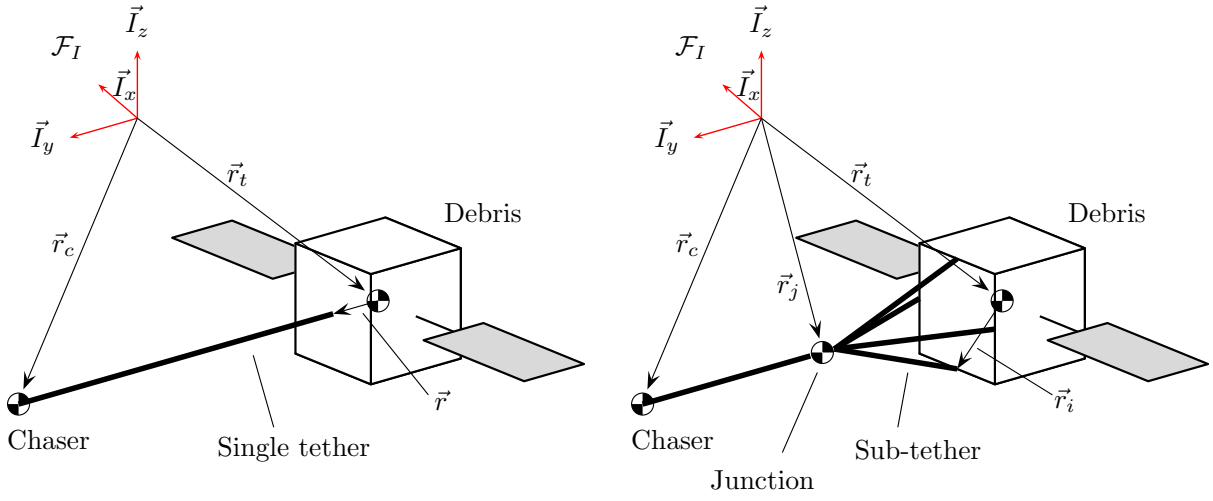

(a) Single tether configuration

(b) Sub-tether configuration

Figure 1. Reference frame and vector definition for dynamics modeling.

$$\mathbf{J}\dot{\boldsymbol{\omega}} + \boldsymbol{\omega}^{\times}(\mathbf{J}\boldsymbol{\omega}) = \boldsymbol{\tau} \tag{4}$$

where $\boldsymbol{\omega}$ is the components of the angular rate vector in $\mathcal{F}_B$, and $\boldsymbol{\tau}$ is the external torque applied to the target.

Assuming that the target body-fixed frame, $\mathcal{F}_B$, is aligned with the principal axis of the body, the target inertia matrix, denoted as J, is represented by:

$$\mathbf{J} = \begin{bmatrix} J_{xx} & 0 & 0 \\ 0 & J_{yy} & 0 \\ 0 & 0 & J_{zz} \end{bmatrix} \tag{5}$$

where J_{xx}, J_{yy}, and J_{zz} are the principal moments of inertia of the target debris.

The attitude of the target is described by quaternion kinematics, given by:

$$\dot{\mathbf{q}} = \frac{1}{2}\mathbf{q}\boldsymbol{\omega} \tag{6}$$

where, $\mathbf{q}$ represents the quaternion describing the attitude of $\mathcal{F}_B$ with respect to $\mathcal{F}_I$ and is defined as:

$$\mathbf{q} = \begin{bmatrix} q_1 \\ q_2 \\ q_3 \\ q_4 \end{bmatrix} = \begin{bmatrix} \mathbf{b}\cos(\frac{\phi}{2}) \\ \sin(\frac{\phi}{2}) \end{bmatrix} \tag{7}$$

where $\mathbf{b}$ is the axis of rotation and ϕ is the angle of rotation.[18]

The inverse square law of the gravitational field of the Earth creates perturbation torques on a body, that are significant in low-Earth orbit. The unequal gravitational force acting across the body leads to restoring torques on the spacecraft.[18] The effect is quantified through:

$$\boldsymbol{\tau}_g = \frac{3\mu}{\|\mathbf{r}_t^b\|^5}\mathbf{r}_t^{b\times}\mathbf{J}\mathbf{r}_t^b \tag{8}$$

where $\boldsymbol{\tau}_g$ is the resulting gravity gradient torque components in $\mathcal{F}_B$, and $\mathbf{r}_t^b$ is the components of the target position vector expressed in $\mathcal{F}_B$, via

$$\mathbf{r}_t^b = \mathbf{A}(\mathbf{q})\mathbf{r}_t.$$

The rotation matrix $\mathbf{A}(\mathbf{q})$ represents a rotation from $\mathcal{F}_I$ to $\mathcal{F}_B$, which is obtained from the quaternion through:

$$\mathbf{A}(\mathbf{q}) = \begin{bmatrix} 1-2q_2^2-2q_3^2 & 2(q_1q_2+q_4q_3) & 2(q_1q_3-q_4q_2) \\ 2(q_1q_2-q_4q_3) & 1-2q_1^2-2q_3^2 & 2(q_2q_3+q_4q_1) \\ 2(q_1q_3+q_4q_2) & 2(q_2q_3-q_4q_1) & 1-2q_1^2-2q_2^2 \end{bmatrix}. \tag{9}$$

B. Translational Motion

To model the target, junction, and chaser linear motion, Newton's second law is used:

$$\mathbf{F} = m\mathbf{a} \tag{10}$$

where $\mathbf{F}$ is the net inertial external force applied to the body, m is the mass of the body, and $\mathbf{a}$ is the inertial linear acceleration.

In the TSS shown in Figure 1b, the main tether and sub-tethers are generating external forces that are applied to each mass. The tether is modeled as a simple spring-damper system, as shown in Figure 2. Defining the i^{th} sub-tether under analysis by the vector $\vec{L}_i$ in $\mathcal{F}_I$ as having components of:

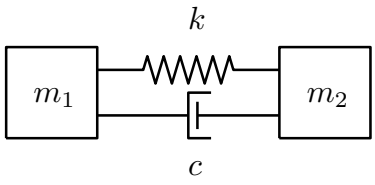

Figure 2. Simple spring-damper system, where two masses are attached via a spring and damper in parallel.

$$\mathbf{L}_i = \mathbf{r}_j - \mathbf{r}_t - \mathbf{A}(\mathbf{q})^{\mathrm{T}}\mathbf{r}_i, \qquad \forall\ i = 1, ..., 4 \tag{11}$$

where $\mathbf{r}_i$ is the attachment point of the i^{th} sub-tether to the target, with respect the the center of the target, in $\mathcal{F}_B$. Treating the linear spring and damper in parallel, the resultant tensile force magnitude developed by the i^{th} sub-tether is:

$$F_i = \begin{cases} k(\|\mathbf{L}_i\| - L_0) + c[\mathbf{v}_j - (\mathbf{v}_t + \mathbf{A}(\mathbf{q})^{\mathrm{T}}\boldsymbol{\omega}^{\times}\mathbf{r}_i)]\frac{\mathbf{L}_i}{\|\mathbf{L}_i\|}, & \text{for } \|\mathbf{L}_i\| - L_0 > 0 \\ 0, & \text{otherwise} \end{cases} \tag{12}$$

where $\mathbf{v}_j$ and $\mathbf{v}_t$ are velocity components of the junction and target in $\mathcal{F}_I$, respectively. The tether material is assumed to have a linear spring constant, k, damping coefficient, c, and unstretched length L_0.

The gravitational force on an orbiting satellite is described by Newton's law of gravitation:

$$\mathbf{F}_g = -\frac{\mu m}{\|\mathbf{r}\|^3}\mathbf{r} \tag{13}$$

where μ is the gravitational parameter of the earth, m is the mass of the orbiting satellite, $\mathbf{r}$ is the components of the position vector of the orbiting satellite in $\mathcal{F}_I$, and $\mathbf{F}_g$ is the resulting force vector components. Newton's law of gravitation applies to the chaser, junction, and target components of the TSS.

C. Equations of Motion

To properly model the motion, all forces contributing to translational motion are included in Eq. (10) for each body. The chaser and junction are treated as point masses, so the effects of external torques are modeled using Eq. (4) for the target only.

The resulting net force on the target debris in $\mathcal{F}_I$ is due to the four sub-tethers and the gravitational effects, and is given by:

$$\mathbf{F}_t = \mathbf{F}_s + \mathbf{F}_g = \sum_1^4 F_i \frac{\mathbf{L}_i}{\|\mathbf{L}_i\|} - \frac{\mu m_t}{\|\mathbf{r}_t\|^3}\mathbf{r}_t. \tag{14}$$

Similarly, for the chaser spacecraft, with the addition of its own thrust force, $\mathbf{F}_{thrust}$

$$\mathbf{F}_c = \mathbf{F}_m + \mathbf{F}_g + \mathbf{F}_{thrust} = F_m \frac{\mathbf{L}_m}{\|\mathbf{L}_m\|} - \frac{\mu m_c}{\|\mathbf{r}_c\|^3}\mathbf{r}_c + \mathbf{F}_{thrust} \tag{15}$$

where, F_m denotes the force magnitude present in the main tether and $\mathbf{L}_m$ denotes its vector components. The junction experiences similar forces:

$$\mathbf{F}_j = \mathbf{F}_s + \mathbf{F}_m + \mathbf{F}_g = \sum_1^4 F_i \frac{\mathbf{L}_i}{\|\mathbf{L}_i\|} + F_m \frac{\mathbf{L}_m}{\|\mathbf{L}_m\|} - \frac{\mu m_j}{\|\mathbf{r}_j\|^3}\mathbf{r}_j. \tag{16}$$

The torque imparted on the target is the sum of the four sub-tether contributions and the gravity gradient effects, given by:

$$\boldsymbol{\tau}_t = \boldsymbol{\tau}_s + \boldsymbol{\tau}_g = \mathbf{A}(\mathbf{q}) \sum_1^4 F_i \frac{\mathbf{r}_i^{\times}\mathbf{L}_i}{\|\mathbf{L}_i\|} + \frac{3\mu}{\|\mathbf{r}_t^b\|^5}\mathbf{r}_t^{b\times}\mathbf{J}\mathbf{r}_t^b \tag{17}$$

which is defined in $\mathcal{F}_B$. To simulate the dynamics, Eqs. (14) to (17) are solved numerically with Eqs. (4) and (10).

IV. Dynamics Formulation - Single Tether Configuration

The dynamics equations for the single tether configuration are very similar to the sub-tether configuration. The major difference is the absence of the junction point, as shown in Figure 1. Therefore, instead of Eq. (11), the tether vector components in $\mathcal{F}_I$ becomes

$$\mathbf{L} = \mathbf{r}_c - \mathbf{r}_t - \mathbf{A}(\mathbf{q})^{\mathrm{T}}\mathbf{r}. \tag{18}$$

Here, $\mathbf{r}$ is the single tether contact point on the target with respect to the centre of the target, as shown in Figure 1a. The force in the tether is:

$$F = \begin{cases} k(\|\mathbf{L}\| - L_0) + c[\mathbf{v}_c - (\mathbf{v}_t + \mathbf{A}(\mathbf{q})^{\mathrm{T}}\boldsymbol{\omega}^{\times}\mathbf{r})]\frac{\mathbf{L}}{\|\mathbf{L}\|}, & \text{for } \|\mathbf{L}\| - L_0 > 0 \\ 0, & \text{otherwise.} \end{cases} \tag{19}$$

The resulting forces and torques on each body are:

$$\mathbf{F}_t = \mathbf{F}_m + \mathbf{F}_g = F\frac{\mathbf{L}}{\|\mathbf{L}\|} - \frac{\mu m_t}{\|\mathbf{r}_t\|^3}\mathbf{r}_t \tag{20}$$

for the force on the target,

$$\mathbf{F}_c = \mathbf{F}_m + \mathbf{F}_g + \mathbf{F}_{thrust} = F\frac{\mathbf{L}}{\|\mathbf{L}\|} - \frac{\mu m_c}{\|\mathbf{r}_c\|^3}\mathbf{r}_c + \mathbf{F}_{thrust} \tag{21}$$

for the force on the chaser, and

$$\boldsymbol{\tau}_t = \boldsymbol{\tau}_m + \boldsymbol{\tau}_g = \mathbf{A}(\mathbf{q})F\frac{\mathbf{r}^{\times}\mathbf{L}}{\|\mathbf{L}\|} + \frac{3\mu}{\|\mathbf{r}_t^b\|^5}\mathbf{r}_t^{b\times}\mathbf{J}\mathbf{r}_t^b \tag{22}$$

for the torque on the target. The forces and torques in Eqs. (20) to (22) are solved numerically with Eqs. (4) and (10) in simulation.

V. Numerical Simulations

To determine the improved performance of the proposed novel tethered configuration to control the attitude of an uncooperative and spinning debris, numerical simulations were performed.

Seven cases are presented, comparing the target stabilization ability of the single tether configuration to the sub-tether configuration. The orbital elements for all simulations are listed in Table 1.

Table 1. Orbital elements used to define initial orbit of TSS.

Orbital Element	Value
Semi-major axis	6871 km
Eccentricity	0.001
Right ascension of the ascending node	20 deg
Inclination	60 deg
Argument of perigee	90 deg
True anomaly	60 deg

Each simulation has similar properties and initial conditions, shown in Table 2. The differences between simulation cases are presented in the following subsections. The chaser is in an identical orbit as the target, but is behind the target by 30 meters, except for Cases 2 and 5, where is it behind by 27 meters. This separation distance is simulated by imparting a small difference in true anomaly for the chaser spacecraft.

Table 2. Initial conditions and TSS parameters for simulations.

Parameter	Value	Parameter	Value	Parameter	Value
J_{xx}, $\mathrm{kg}\cdot\mathrm{m}^2$	15000	m_t, kg	3000	Debris Size, m	[1.25,1.75,1.25]
J_{yy}, $\mathrm{kg}\cdot\mathrm{m}^2$	3000	m_j, kg	10	L_{single}, m	30
J_{zz}, $\mathrm{kg}\cdot\mathrm{m}^2$	15000	m_c, kg	500	L_{main}, m	15.0
k, $\frac{\mathrm{kN}}{\mathrm{m}}$	3150	c, $\frac{\mathrm{Ns}}{\mathrm{m}}$	16	L_{sub}, m	15.2

The simulations are performed using an Adams integration scheme over 6000 seconds (approximately one orbit), using a 1 second output time step. Output graphs show the resulting angular rates of the target as a function of time, to determine whether the target is effectively being controlled. The angle between the front-face-normal of the target and the single tether as a function of time, denoted θ as represented in Figure 3, is also presented to show how close the attitude of the target is to its equilibrium point. The proposed sub-tether configuration uses a hypothetical single tether to calculate the angle, such that the two TSS solutions can be readily compared. The tether elongation as a function of time is presented to determine if tether oscillations are present. For consistency, the same tether and target parameters as in Ref. 17 are used.

A. Case 1

A debris is captured at $t = 0$ when it has initial angular rates of:

$$\boldsymbol{\omega} = \begin{bmatrix} 0 \\ 0.05 \\ 0 \end{bmatrix} \frac{\mathrm{rad}}{\mathrm{s}}.$$

The debris is not captured perfectly, however. To simulate this, an initial tether angle of $\pi/6$ radians is applied such that the target is not facing the chaser upon capture. The chaser thrusts 20 N in the retrograde

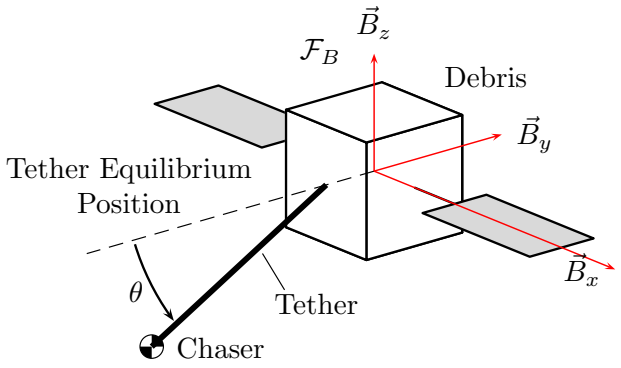

Figure 3. Angle θ represents the current angle between the tether and its equilibrium point. Reference frame $\mathcal{F}_B$ defines the body-fixed reference frame on the target debris.

direction, and is initially 30 meters behind the target in the orbit such that all tethers are initially tight.

This case shows that in the presence of a thrust force on the chaser, the angular rates of the target can be controlled. Figure 4a shows that sub-tether configuration damps the angular rates of the passive target much faster than the single tether configuration. It is interesting to note that neither configuration can control the angular rates about the y axis, due to the lack of a moment arm about the y axis, as defined in Figure 3. This is a limitation of the TSS debris removal solution, in that it cannot control the angular rates of the target about the axis joining the chaser and the target. The angular rates in the x and z axes approach zero, but they do not reach zero. The nature of the sub-tether configuration leads to a non-zero angular separation between when one sub-tether becomes tight and when an opposite sub-tether becomes tight. Therefore, small scale oscillations are expected to be present in the long term. However, simulations modeling the effects of a target captured by a net have shown that the friction between the net and the target will, over time, reduce the angular rates further.[19]

Another measure of the performance of the TSS is to show the angle between the tether and its equilibrium position, as depicted in Figure 3. The sub-tether configuration uses a hypothetical single tether to calculate said angle, such that the target orientation can be compared. The angle is initially at $\pi/6$ to simulate an imperfect capture process. Figure 4b shows that while the angle in the single tether case is decreasing over time, it does so very slowly compared to the sub-tether configuration angle. If the target is always facing the chaser (i.e., a low angle), there are multiple benefits. First, the target will have reduced oscillations. For a piece of debris that has been in orbit for an extended period of time, smaller oscillations may reduce the chance of break up. Second, the desired towing configuration is when the chaser is perfectly aligned with the chaser,[17] so the quicker this configuration can be obtained the more efficient the TSS debris removal solution will be.

Figure 4c shows the tether elongation as a function of time. For the sub-tether scenario, the longest of the four sub-tethers (i.e., the one currently being stretched) is used in the calculation. Again, the sub-tether configuration outperforms the single tether scenario, with lower stretch amplitudes. This shows that there will be lower oscillatory forces in the tether over time. The tether stretch tends towards a constant positive value which is a result of the constant thrust force provided by the chaser.

B. Case 2

A debris is captured at $t = 0$, similar to Case 1. All initial conditions are identical except the chaser is initially 27 meters behind the target. The tethers are still 30 meters long, thereby creating an initial slackness in the tethers of 3 meters. As the chaser thrusts away from the target, there will be an initial jolt when the tethers becomes tight for the first time. Figure 5a shows how the angular rates become damped to their final values nearly as quickly to Case 1. Therefore, Case 2 shows that capturing the target with an initially slack tether leads to a safe stabilization and that the sub-tether TSS configuration is still a better solution to the stabilization of an uncooperative target.

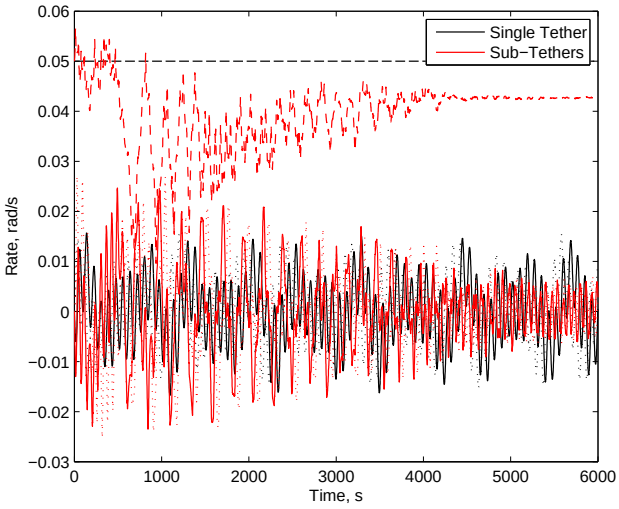

(a) Target angular rates

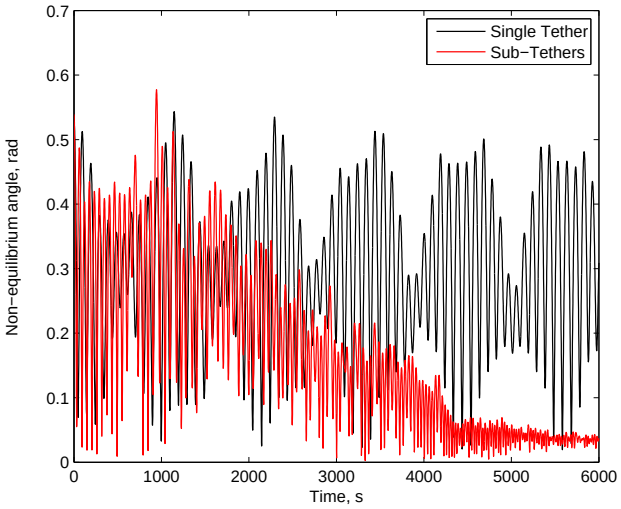

(b) Tether angle

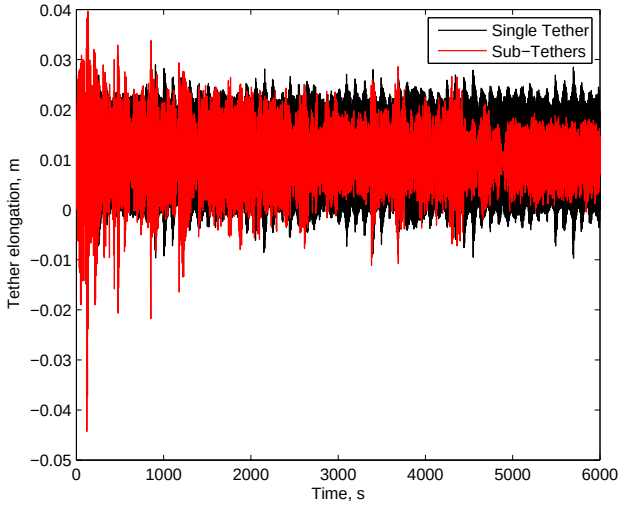

(c) Tether elongation

Figure 4. Resulting TSS motion for Case 1. Dashed lines represent the angular rate about the y-axis, and the dotted and solid lines represent the two transverse axes, as shown in Figure 3.

C. Case 3

Case 3 investigates the effects of a smaller 3 N thrust force from the chaser. This case considers a scenario where the chaser is towing the target with less thrust than was used during the stabilizing process. Here, the target is already facing the chaser, but is continues to have a spin about its minor (and uncontrollable) axis, of:

$$\boldsymbol{\omega} = \begin{bmatrix} 0 \\ 0.05 \\ 0 \end{bmatrix} \frac{\text{rad}}{\text{s}}.$$

Figure 6a shows that as perturbations act on the target, its angular rates about the x and z axes remain small and bounded with either configuration. Figure 6b shows how the tether angle is considerably lower for the sub-tether configuration than the single tether configuration, which allows the target to remain nearer its equilibrium position during the towing. The stretch for the sub-tether configuration, as shown in Figure 6c is constant for the sub-tether configuration. The single tether, however, develops oscillations due to the

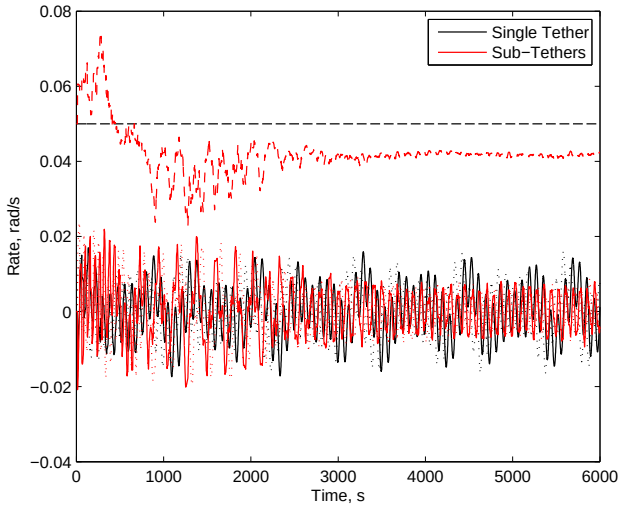

(a) Target angular rates

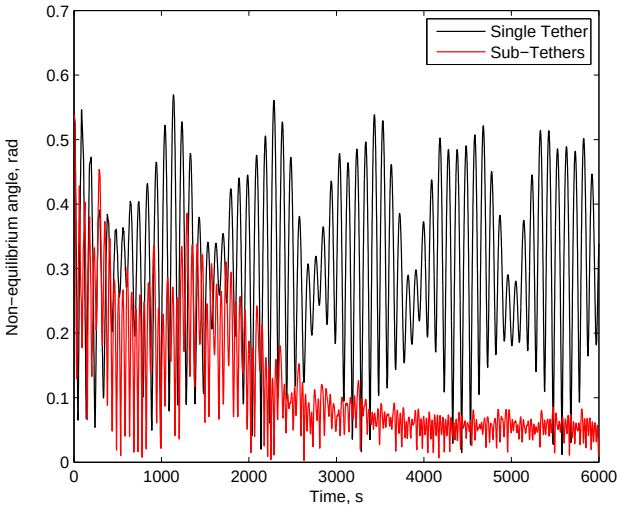

(b) Tether angle

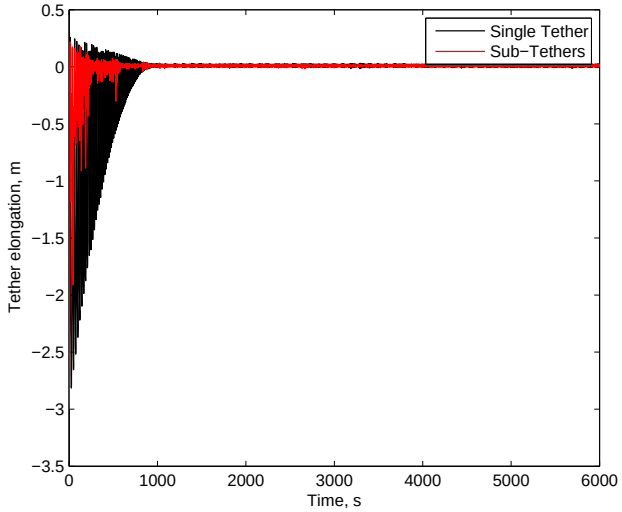

(c) Tether elongation

Figure 5. Resulting TSS motion for Case 2

perturbations which result in slackness of the tether of up to 0.5 meters. Therefore, if the towing phase of the debris removal mission is planning on using a low-thrust engine, the sub-tether configuration is a better option as it keeps the target near its equilibrium position to ensure safe towing.

D. Case 4

Cases 4 - 6 consider the likely possibility of target angular rates about all three axes. Initial angular rates of:

$$\boldsymbol{\omega} = \begin{bmatrix} 0.025 \\ 0.025 \\ 0.025 \end{bmatrix} \frac{\text{rad}}{\text{s}}$$

are used. This case has the target initially facing the chaser (i.e., zero tether angle), 20 N of thrust from the chaser, and 30 meters separation such that all tethers are initially tight. Figure 7 presents the results.

This case is more severe than Cases 1-3 because the target is tumbling with angular rates about all three axes. Figure 7a shows how after one orbit, the angular rates of the target using the sub-tether configuration

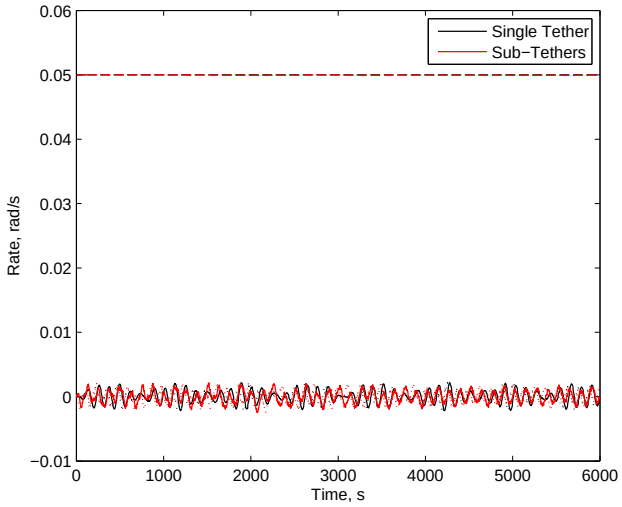

(a) Target angular rates

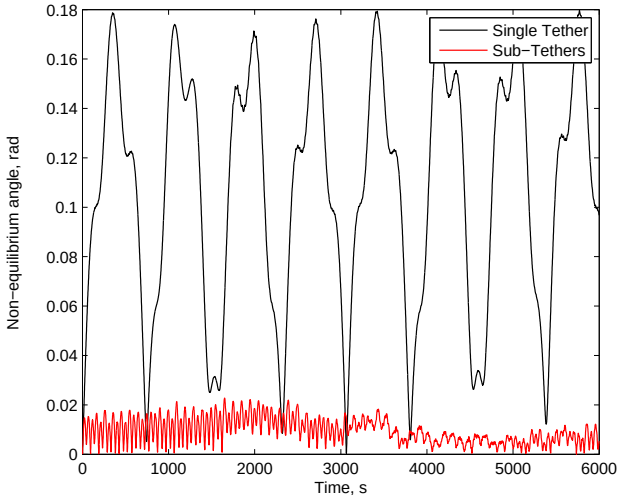

(b) Tether angle

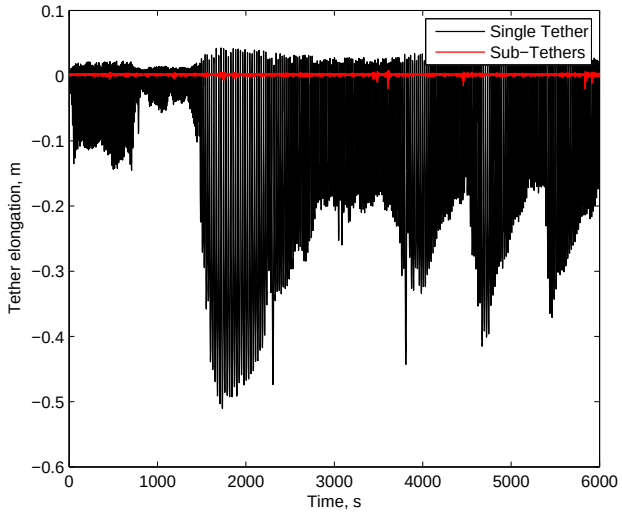

(c) Tether elongation

Figure 6. Resulting TSS motion for Case 3

are significantly reduced compared to the single tether configuration. This is due to the placement of the sub-tether attachment points on the target. By attaching the sub-tethers to the target at its extremities where the relative velocities are highest, as shown in Figure 1b, the damping effect in the sub-tethers is better utilized. Since damping is the only mode of energy dissipation in the system, attaching sub-tethers to the points of highest relative velocity is a more effective method of dissipating the angular momentum of a tumbling debris.

E. Case 5

This case has the same initial conditions as Case 4 except the target is initially offset from the chaser with an angle of $\pi/6$ radians, and the tethers are initially 3 meters slack. Twenty Newtons of thrust is used. This represents one of the worst-case capture scenarios. That is, an imperfect capture with an initial tether angle of $\pi/6$ rads, an initially 3 meter slack tether, and a tumbling target with angular rates about all three axes. Figure 8 once again shows how the sub-tether configuration outperforms the single tether, even in a worst case capture scenario. Both the angular rates, the angular offset, and the tether elongation reach their steady state values much quicker than the single tether TSS, using the same amount of thrust.

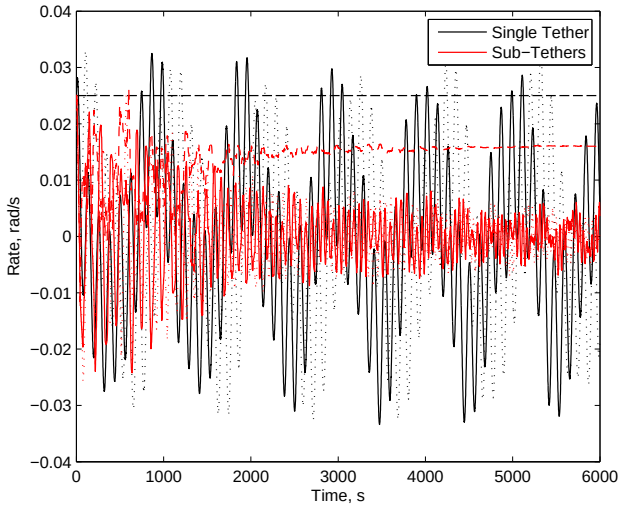

(a) Target angular rates

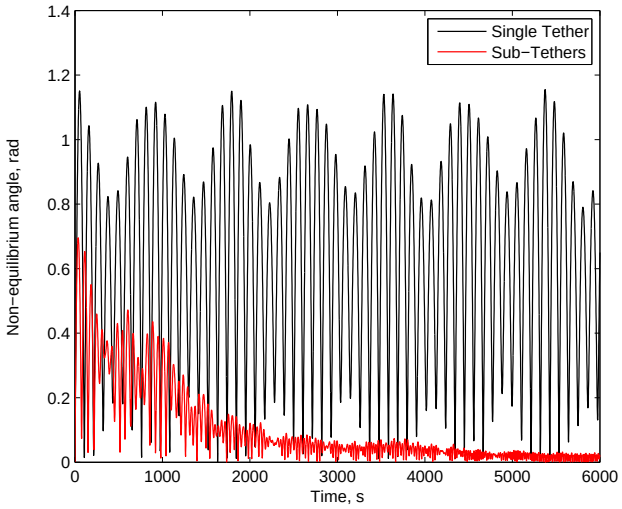

(b) Tether angle

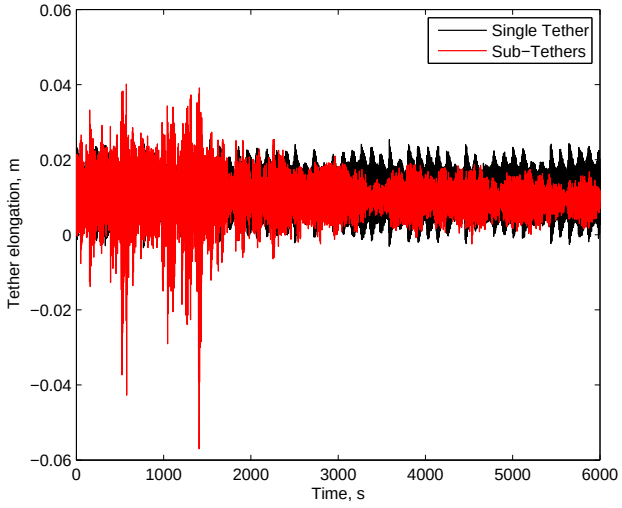

(c) Tether elongation

Figure 7. Resulting TSS motion for Case 4

F. Case 6

Case 6 presents a different approach of controlling the attitude of the target without the use of thrust. Instead, the chaser is given an additional radial velocity of 2 m/s such that the TSS rotates about its centre of mass. The tethers are initially tight, and there is no initial tether angle. This demonstrates another mode for preventing collision and maintaining tension in the tethers sufficient for controlling the attitude of the debris. That is, to rotate the chaser and the debris around each other (i.e., rotating the TSS about its barycenter). Figure 9b shows how after one orbit the tether angle for the sub-tether configuration quickly stabilizes such that the target is very close to its equilibrium position. The single tether configuration has angles after one orbit of 2 radians, indicating very little control of the attitude of the target. The TSS is rotating about its barycentre, so instead of reducing the target angular rates to zero, they will be non-zero and predictable. The sub-tether configuration arrives at its steady state in approximately half an orbit, whereas the single tether configuration will require many more orbits before the barycentre rotation technique has stabilized the target.

As shown in Figure 9a, this case demonstrates another stable mode of motion after capture. That is, a controlled rotation rate along two axes (rather than attempting to bring them to near zero). This

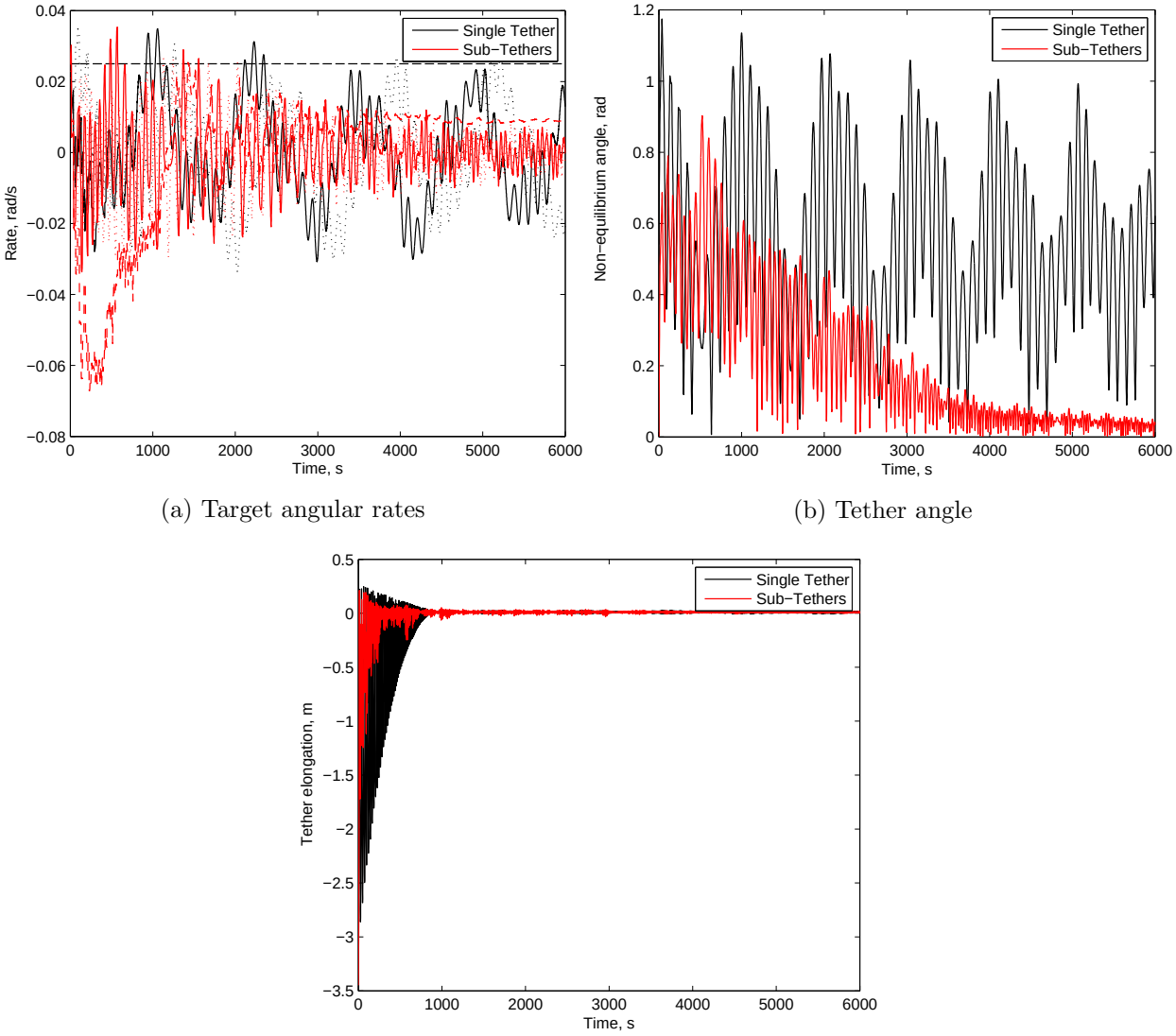

(a) Target angular rates

(b) Tether angle

(c) Tether elongation

Figure 8. Resulting TSS motion for Case 5

yields predictable and passive target attitude motion, once the chaser and target have begun rotating. Safe separation is demonstrated in Figure 9c.

A significant advantage of this control technique is that it does not require any thrust other than that to initiate the spin. This may reduce the complexity of the angular momentum dissipation process.

G. Case 7

This case investigates the motion of the system when the target is already stabilized and the chaser is not using thrust. This simulation provides a sense of the natural tendencies of the system, and is useful when considering the long-term safety of the debris removal system. The simulated target has initially no angular rates or tether angle, the tethers are initially tight, and the chaser is passive. The simulation was performed over two orbits (12000 seconds). Simulation results, in Figure 10, show that the relative motion between the chaser and the target that is induced by the orbital motion does not sustain enough tension in the tethers to maintain attitude control of the target. Gravity gradient perturbations are dominant and control of the target is lost. Tethers can possibly become tangled in this situation. The tethers became 15 meters slack,

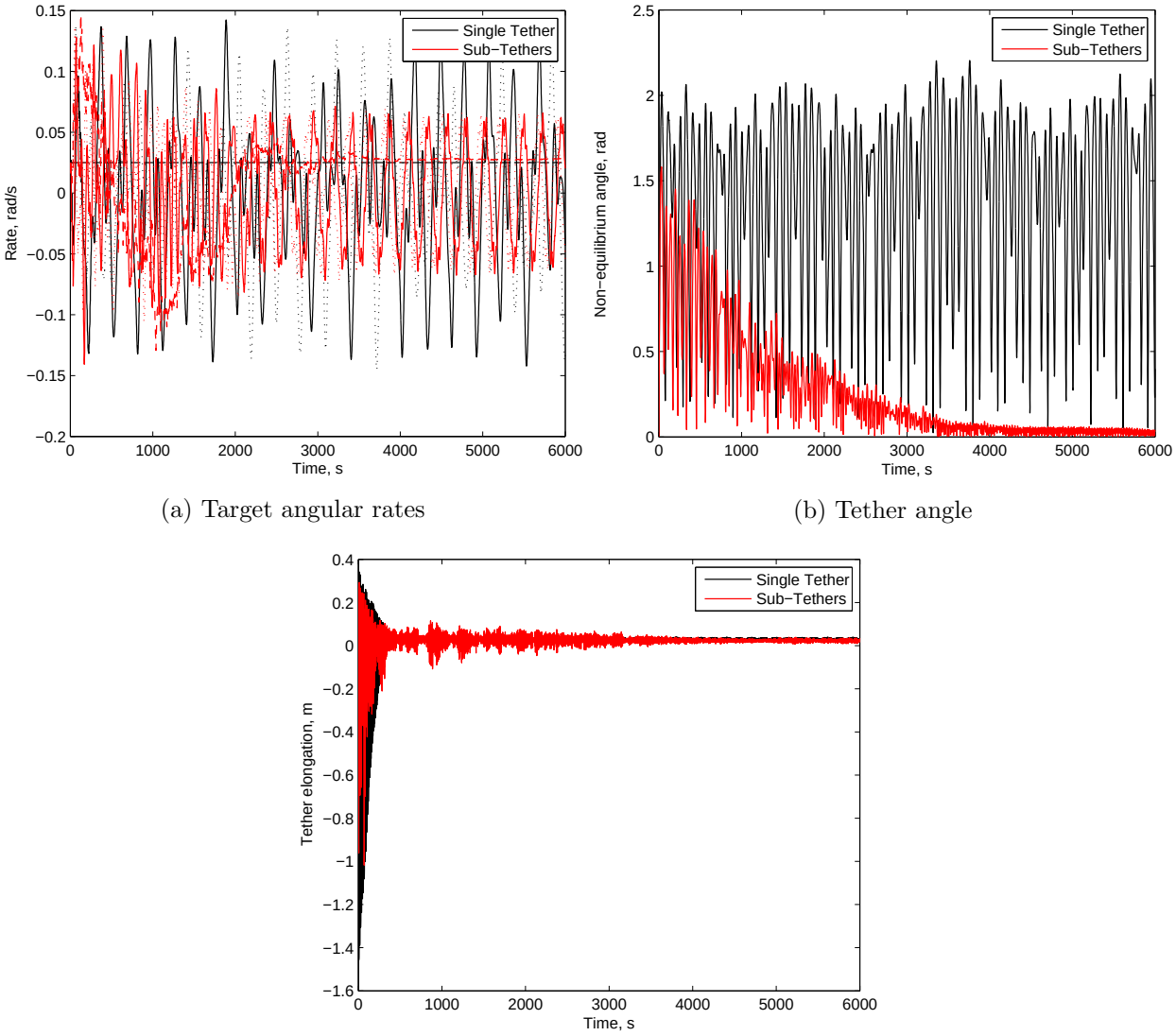

(a) Target angular rates

(b) Tether angle

(c) Tether elongation

Figure 9. Resulting TSS motion for Case 6

which indicates that a collision is possible. Neither TSS configuration maintained control of the target during this simulation, demonstrating the need for chaser control at all times.

VI. Conclusions

A novel Tethered Satellite System (TSS) where a main tether attached to the chaser branches into four sub-tethers that are attached to a tumbling passive satellite was proposed, analyzed and compared to the previously accepted TSS configuration that has a single tether joining the two spacecraft. An orbital environment was simulated, and included orbital motion and gravity gradient torques. Seven simulation cases were performed, each demonstrating a different capture scenario, for both the sub-tether TSS and the single tether TSS.

Cases 1-5 used thrust on the chaser spacecraft to thrust in the opposite direction to the target. In these scenarios, the thrust maintained sufficient tension in the tethers to prevent collision and regulate the angular momentum of the target. After one orbit, the resulting motion of the sub-tether TSS and the single tether TSS was compared. In these five cases, the sub-tether configuration lead to a nearly stabilized target (i.e.,

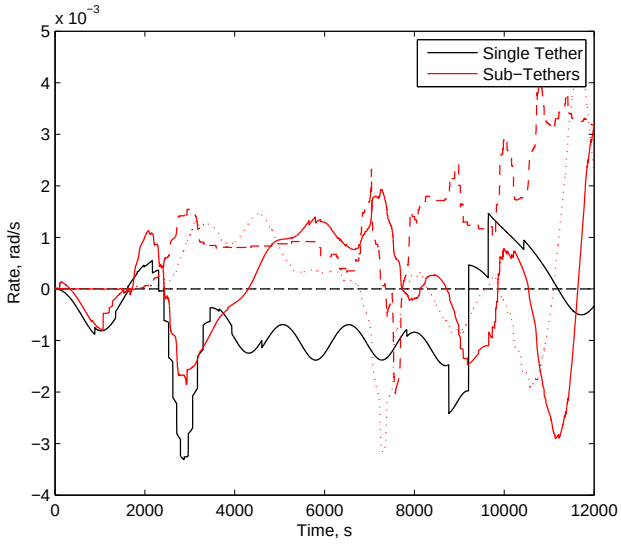

(a) Target angular rates

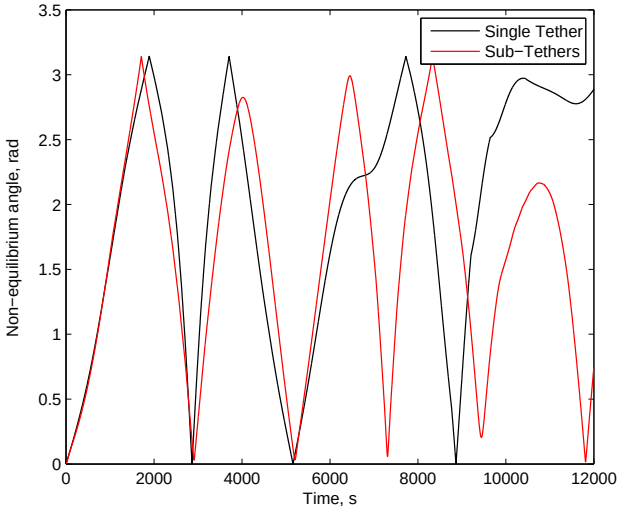

(b) Tether angle

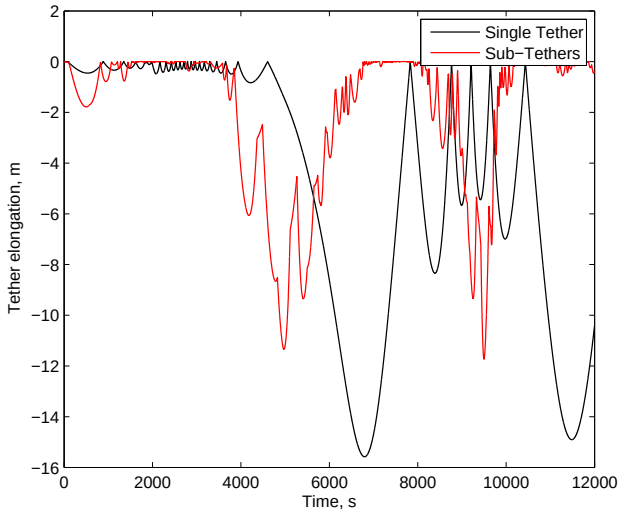

(c) Tether elongation

Figure 10. Resulting TSS motion for Case 7

low transverse angular rates, and a low tether angle), ideal for transporting the target to its disposal orbit. The single tether configuration, however, did not. After one orbit, the angular rates and tether angle were still large. Attempting to transport an un-stabilized target will result in control difficulties for the chaser, and in turn, require more fuel and a more expensive mission. Cases 1-5 shows that all else being equal, the novel sub-tether TSS proposed in this paper always leads to a significantly more stable target than the single tether configuration.

Case 6 demonstrated a capture scenario where the TSS is spun around its barycentre. The goal is to use the centripetal force generated in the tethers to stabilize the target, rather than use thrust on the chaser to achieve the same effect. Again, the sub-tether configuration leads to a more stable target in the same amount of time than the single tether configuration. It was demonstrated that capturing a debris in this manner could quickly stabilize a target and not require any fuel, other than that to initiate the spin.

Case 7 showed that a passive chaser should be avoided, as a collision or tether tangling could readily occur for either configuration. If a passive, safe, long-term configuration is desirable, it is recommended to initiate a barycentre rotation.

An important result from all the simulation cases is the angular momentum along the main tether axis (i.e., the y axis as shown in Figure 3) cannot be controlled, no matter what TSS configuration is used. This is due to the lack of a moment arm about this axis and the flexible nature of the tether material. If a mission were being designed to capture a tumbling debris, this result indicates that the debris should be approached along its axis of least angular momentum.

Future work will focus on the inclusion of the frictional effects between the target and the net, and experimentation to determine realistic tether damping coefficients. To validate the dynamics simulation results, three degree-of-freedom experiments using free-floating air-bearing spacecraft platforms maneuvering on a large granite surface at the Spacecraft Robotics and Control Laboratory at Carleton University will be performed.

Acknowledgments

This research was financially supported in part by the Natural Sciences and Engineering Research Council of Canada under the Canadian Graduate Student - Masters scholarship.

References

[1]Kessler. D.J., and Cour-Palais, B.G., "Collision Frequency of Artificial Satellites: The Creation of a Debris Belt," *Journal of Geophysical Research*, Vol. 83, No. A6, 1978, pp. 2637-2646.

[2]Wormnes, K., Le Letty, R., Summerer, L., Schonenborg, R., Dubois-Matra, O., Luraschi, E., Cropp, A., Krag, H., and Delaval, J. "ESA technologies for space debris remediation," *6th International Association for the Advancement of Space Safety Conference: Safety is Not an Option*, Montreal, Canada, 2013.

[3]Shan, M., Guo, J., Gill, E., "Review and comparison of active space debris capturing and removal methods," *Progress in Aerospace Sciences* (to be published).

[4]Reintsema, D., Thaeter, J., Rathke, A., Naumann, W., Rank, P., Sommer, J., "DEOS the German robotics approach to secure and de-orbit malfunctioned satellites from low earth orbits," *International Symposium on Artificial Intelligence, Robotics and Automation in Space*, Sapporo, Japan, 2010.

[5]Lavagna, M., Armellin, R., Bombelli, A., Benvenuto, R., "Debris removal mechanism based on tethered nets," *International Symposium on Artificial Intelligence, Robotics and Automation in Space*, Turin, Italy, 2012.

[6]Ohkawa, Y., Kawamoto, S., Nishida, S., and Kitamura, S., "Research and Development of Electrodynamic Tethers for Space Debris Mitigation," *Transactions of the Japan Society for Aeronautical and Space Sciences*, Vol. 7, No. ists26, 2009.

[7]Jasper, L. E. Z., Seubert, C.R., Schaub, H., Valery, T., and Yutkin, E., "Tethered Tug for Large Low Earth Orbit Debris Removal," *AAS/AIAA Astrodynamics Specialists Conference*, Charleston, SC, 2012, AAS Paper 12-252.

[8]Kaplan, M.H., Boone, B., Brown, R., Criss, T.B., and Tunstel, E.W., "Engineering Issues for All Major Modes of In Situ Space Debris Capture," *AIAA Space 2010 Conference & Exposition*, Anaheim, CA, 2010, AIAA Paper 2010-8863.

[9]Alpatov, A. P., Beletsky, V. V., Dranovskii, V. I., Khoroshilov, V. S., Pirozhenko, A. V., Troger, H., and Zakrzhevskii, A. E., *Dynamics of Tethered Space Systems*, Taylor & Francis, Boca Raton, FL, 2010.

[10]Cosmo, M. L., and Lorenzini, E. C., *Tethers in Space Handbook*, Smithsonian Astrophysical Observatory, 1997.

[11]Johnson, L., Gilchrist, B., Estes, R. D., and Lorenzini, E., "Overview of future NASA tether applications," *Advances in Space Research*, Vol. 24, No. 8, 1999.

[12]Chen, Y., Huang, R., Ren, X., He, L., and He, Y., "History of the Tether Concept and Tether Missions: A Review," *ISRN Astronomy and Astrophysics*, 2013.

[13]Aslanov, V. S. and Yudintsev, V. V., "Dynamics of large debris connected to space tug by a tether," *Journal of Guidance, Control and Dynamics*, Vol. 36, No. 6, 2013, pp. 1654-1660.

[14]Aslanov, V. S., and Yudintsev, V. V., "Dynamics, Analytical Solutions and Choice of Parameters for Towed Space Debris with Flexible Appendages," *Advances in Space Research* Vol. 55, 2015, pp. 660-667.

[15]Aslanov, V. S., and Yudintsev, V. V., "Behavior of Tethered Debris With Flexible Appendages," *Acta Astronautica*, Vol. 104, No. 1, 2014, pp. 91-98.

[16]Aslanov, V. S., and Ledkov, A. S. "Dynamics of Towed Large Space Debris Taking Into Account Atmospheric Disturbance," *Acta Mechanica*, Vol. 225, No. 9, 2014, pp. 2685-2697.

[17]Aslanov, V. S., and Yudintsev, V. V., "Dynamics of Large Space Debris Removal Using Tethered Space Tug," *Acta Astronautica*, Vol. 91, 2013, pp. 149-156.

[18]Hughes, P., *Spacecraft Attitude Dynamics*. Dover Publications, Mineola, NY, 2004, pp. 17-18, 58-59, 233-239.

[19]Benvenuto, R., Salvi, S. and Lavagna, M., "Net Capturing of Tumbling Space Debris: Contact Modeling Effects on the Evolution of Disposal Dynamics," *13th Symposium on Advanced Space Technologies in Robotics and Automation*, Noordwijk, The Netherlands, 2015.

[20]Levin, E. M., "Dynamic Analysis of Space Tether Missions," *Advances in the Astronautical Sciences*, Vol. 126, 2007.